

Article

# Liquid-Filled Highly Asymmetric Photonic Crystal Fiber Sagnac Interferometer Temperature Sensor

Yashar E. Monfared <sup>1,\*</sup>, Amir Ahmadian <sup>2</sup>, Vigneswaran Dhasarathan <sup>3,4</sup> and Chunhao Liang <sup>5,\*</sup><sup>1</sup> Department of Chemistry, Dalhousie University, Halifax, NS B3H 4R2, Canada<sup>2</sup> Department of Electrical and Computer Engineering, Science and Research Branch, Azad University, Tehran 147789385, Iran; amir.ahmadian@ieee.org<sup>3</sup> Division of Computational Physics, Institute for Computational Science, Ton Duc Thang University, Ho Chi Minh City 700000, Vietnam; vigneswaran.d@tdtu.edu.vn<sup>4</sup> Faculty of Electrical and Electronics Engineering, Ton Duc Thang University, Ho Chi Minh City 700000, Vietnam<sup>5</sup> Shandong Provincial Engineering and Technical Center of Light Manipulations & Shandong Provincial Key Laboratory of Optics and Photonic Device, School of Physics and Electronics, Shandong Normal University, Jinan 250014, China

\* Correspondence: y.monfared@dal.ca (Y.E.M.); cliang@dal.ca (C.L.)

Received: 26 March 2020; Accepted: 15 May 2020; Published: 19 May 2020



**Abstract:** In this paper, we theoretically designed and numerically studied a high-resolution and ultrasensitive photonic crystal fiber temperature sensor by selective filling of a liquid with high thermo-optic coefficient in one of the airholes of the fiber. The finite element method was utilized to study the propagation characteristics and the modal birefringence of the fiber under different ambient temperatures. A large base birefringence value of  $7.7 \times 10^{-4}$  as well as a large birefringence sensitivity of almost 29% to a 10 °C temperature variation was achieved for the optimized fiber design with liquid chloroform between 15 °C and 35 °C. We also studied the performance of the proposed optical fiber in a temperature sensing Sagnac interferometer. An average linear temperature sensitivity of 17.53 nm/°C with an average resolution of  $5.7 \times 10^{-4}$  °C was achieved over a temperature range of 20 °C (15 °C to 35 °C).

**Keywords:** fiber-optic temperature sensor; chloroform fiber; Sagnac interferometer

## 1. Introduction

Optical properties and applications of photonic crystal fibers (PCFs), either as a nonlinear medium for nonlinear optics or as an optical functional device such as a sensor, have been the focus of intense research in recent years [1–4]. Comparing to conventional optical fibers, PCFs demonstrate important characteristics including design flexibility, controllable effective area, adjustable dispersion, and the potential to achieve a highly birefringent structure to confine light [1–3]. The regular PCFs made from silica are not sensitive to temperature as silica does not exhibit a large thermo-optic coefficient [4]. However, the design flexibility of PCFs can assist scientists to increase the temperature sensitivity of the fiber via liquid infiltration into the fiber holes [4].

Most of the liquids exhibit a large thermo-optic coefficient (TOC). A large TOC can be used to realize various effective mode indices of the fundamental guided mode in the fiber infiltrated with liquids at different temperatures [4]. By introducing an asymmetry in the fiber structure, the mode indices will also be sensitive to the polarization of the light, which can enable us to design highly birefringent PCFs [5]. By simultaneously infiltrating the PCF and introducing asymmetry in the design of the fiber, one can design an optical fiber that is sensitive to both the temperature and the polarization of the light. An interferometric technique, like Sagnac interferometry, can be used to detect changes in

the light transmission spectrum in a fiber loop depending on the fiber birefringence [4,6]. Therefore, one can use a highly birefringent PCF in a fiber-loop Sagnac interferometer as a tool for accurate temperature sensing in hard-to-reach environments.

There have been multiple studies on the properties of selectively liquid-filled PCF temperature sensors based on interferometric techniques. Qian et al. [7] proposed an alcohol-filled PCF temperature sensor with a sensitivity of 6.6 nm/°C. Lu et al. [8] proposed a temperature sensor based on a PCF filled with silver nanowires and liquid, and they achieved a sensitivity of 2.7 nm/°C. Cui et al. [6] proposed a selectively water-filled PCF based on Sagnac interferometry with a sensitivity of 2.58 nm/°C. Han et al. [9] reported a selective-filling PCF by infiltrating a liquid into two adjacent air holes of the innermost ring of holes, and a temperature sensitivity of around −10.0 nm/°C was achieved. Recently, Vera et al. [10] proposed a metal-filled PCF for a Sagnac interferometry temperature sensor with a sensitivity of −9 nm/°C. Monfared et al. [4] also studied a toluene-filled PCF temperature sensor via a Sagnac interferometer with a sensitivity of −11 nm/°C and a temperature range of 20–30°C.

In this paper, we study a simple PCF structure with only two rings of air holes and two smaller modified holes, filled with fluid as a temperature-sensitive material and close to the core of the fiber. We also study the design parameters and performance of the proposed temperature sensor in different temperatures and demonstrate the possibility of temperature sensing with measuring the variations in the transmission spectrum of the fiber.

## 2. Sensor Design

### 2.1. Materials and Methods

In the PCF structure, we used silica as the background material (core and cladding), two rings of air holes with diameter  $d$  and center-to-center spacing  $\Lambda_2$ , and two modified-location holes ( $\Lambda_1 = 1.5 \Lambda_2$ ) with diameters  $D_1$  and  $D_2$ . The larger hole is filled with liquid chloroform. We simulated the PCF structure using the finite element method (FEM) applied with the COMSOL Multiphysics software. Perfectly matched layer (PML) boundary conditions as well as ultrafine mesh size with a minimum element size of 5 nm and a maximum element size of 500 nm were applied to the model. Furthermore, strict convergence analyses were conducted to ensure the accuracy of the results (error threshold of  $10^{-5}$ ). The cross section of the proposed PCF is shown on Figure 1a. It should be noted that only two rings of airholes will be an advantage during the fabrication process of the PCF, as having fewer rings with low filling ratios ( $d/\Lambda$  and  $D/\Lambda$ ) is technologically easier and can significantly reduce fabrication-induced imperfections [5].

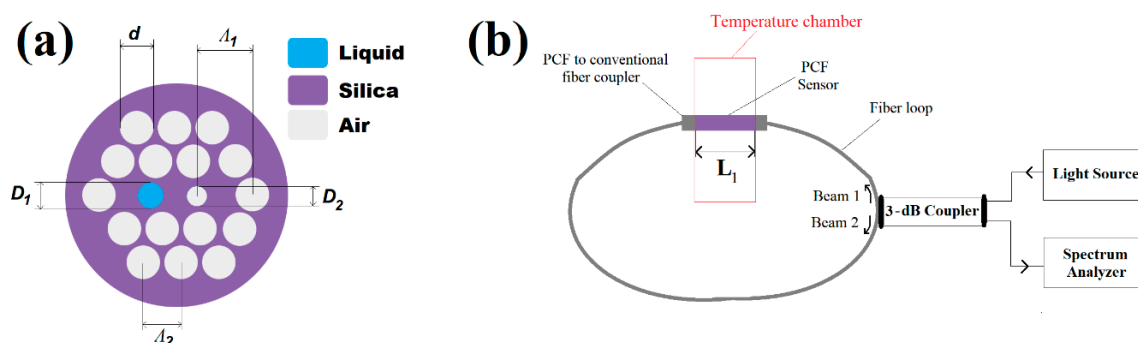


**Figure 1.** (a) Cross section of the selectively liquid-filled photonic crystal fibers (PCF) with hole diameter  $d$ , two modified-position holes with diameters  $D_1$  and  $D_2$ , modified-location hole pitch  $\Lambda_1$ , and nonmodified-location hole pitch  $\Lambda_2$ . (b) The schematic of the potential experimental setup of the PCF sensor in a Sagnac interferometer.

In Figure 1b, we also demonstrate a possible experimental setup for our sensor. The mechanism of a Sagnac-interferometer-based optical fiber sensor is based on the phase difference of light beams

that propagate through the fiber loop which was described in [4,6]. In summary, a laser source emits an optical beam, which is split into two beams using a beam splitter or a 3-dB optical coupler [9,10]. These beams (beam 1 and beam 2) counter-propagate through a fiber loop that usually consists of a conventional optical fiber with a negligible loss at operation wavelengths close to 1200 nm [4,6]. The beams recombine at the output while undergoing a phase difference (as a result of a different optical path lengths) which is caused by a temperature-sensitive birefringence value of the sensing element (the proposed birefringent chloroform-filled optical fiber) during propagation in the fiber loop.

There are numerous methods to fill the holes of the PCF with liquids, including the photo-lithographic masking technique [11] and utilizing different flow speeds of the liquids [12], which already are taken into practice. As our fiber cross section is relatively large (larger than 10 μm), its coupling efficiency with conventional optical fibers can be as large as 90% using an appropriate coupler—for example, the fused biconical tapering technique [13], which makes the propagation of light possible in the prospective setup. Furthermore, the previous tests on liquid-filled Sagnac interferometer fiber sensors show consistent, accurate, and stable results [6,14], which makes the proposed sensor a potential candidate in many industrial applications.

### 2.2. Optical Materials

We started by comparing the thermo-optic coefficient (TOC) of different liquids. A liquid with a high TOC shows a large variation in refractive index as a function of temperature, which can be utilized to design a highly sensitive temperature sensor. The TOC values are obtained from [15,16], and they are close to our operation wavelengths in visible and near infrared regions. As seen in Figure 2, liquid chloroform (CHCl<sub>3</sub>) and carbon disulfide (CS<sub>2</sub>) show the most promising TOC values. While chloroform and CS<sub>2</sub> have the highest TOCs, chloroform has lower linear and nonlinear refractive indices than CS<sub>2</sub> (nearly 1.435 and 85 × 10<sup>-20</sup> m<sup>2</sup>/W, compared to 1.585 and 320 × 10<sup>-20</sup> m<sup>2</sup>/W of CS<sub>2</sub>), which help with suppressing unwanted nonlinear processes and nonlinearity in the sensing performance of the fiber [17]. Therefore, chloroform has a greater overall merit compared to other liquids for the temperature sensing application proposed here, and for this reason we used chloroform in our proposed sensor and all simulations.

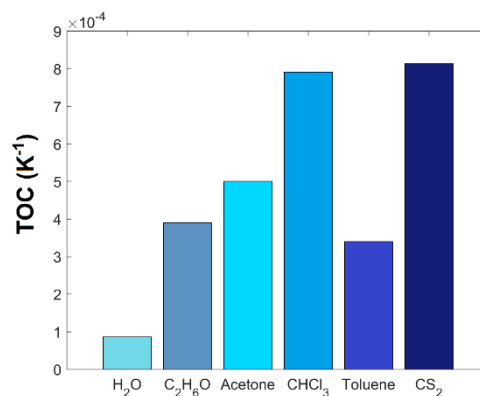


**Figure 2.** The magnitude of the thermo-optic coefficient of different liquids close to the operation wavelengths. H<sub>2</sub>O is water, C<sub>2</sub>H<sub>6</sub>O is ethanol, CHCl<sub>3</sub> is chloroform, and CS<sub>2</sub> is carbon disulfide.

In our simulations, we considered the material dispersion of silica and chloroform to accurately simulate the resulting structure. The relationship between the refractive index of silica and the wavelength is given by the following Sellmeier’s equation [18,19]:

$$n_{silica}^2 = 1 + \frac{0.6961663\lambda^2}{\lambda^2 - 0.0684043^2} + \frac{0.4079426\lambda^2}{\lambda^2 - 0.1162414^2} + \frac{0.8974794\lambda^2}{\lambda^2 - 9.896161^2} \tag{1}$$

where  $\lambda$  is the wavelength of incident light. The relationship between the refractive index of liquid chloroform, wavelength, and temperature is given by the following equation [20]:

$$n_{chloroform}(\lambda, T) = n_{chloroform@20}(\lambda) + (\Delta T dn_T) \tag{2}$$

Here,  $T$  is the temperature in Celsius;  $\Delta T$  is the difference between 20 °C and the chosen temperature;  $dn_T$  is the rate of variation in refractive index as a function temperature, which is equal to  $-7.91 \times 10^{-4} \text{ K}^{-1}$ ; and  $n_{chloroform@20}(\lambda)$  is the refractive index of chloroform as a function of wavelength at 20 °C, which is given by the following Sellmeier’s equation [20]:

$$n_{chloroform@20}(\lambda) = 1.431364 + \frac{5632.41}{\lambda^2} - \frac{2.0805 \times 10^8}{\lambda^4} + \frac{1.2613 \times 10^{13}}{\lambda^6} \tag{3}$$

In Figure 3, we can see the relationship between the ambient temperature and the refractive index of chloroform for different temperatures ranging from 20 °C to 30 °C with different excitation wavelengths.

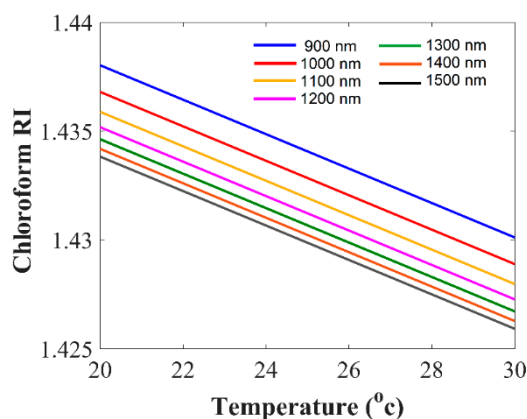


Figure 3. Chloroform refractive index as a function of temperature for different excitation wavelengths.

Finally, we considered the refractive index of air to be 1. This completes our numerical model for simulations in the proposed chloroform-filled PCF.

### 2.3. Birefringence and Sagnac Interferometry

The key parameter for an optical fiber in a Sagnac interferometer is birefringence ( $B$ ), which is defined in [4] as

$$B = n_{fast} - n_{slow}, \tag{4}$$

where  $n_{fast}$  and  $n_{slow}$  are the effective mode indices of the two orthogonal states of the fundamental guided mode in the fiber core. In a birefringence fiber, the effective modal indices of these orthogonally polarized modes differ significantly. Here, a FEM analysis applied with Comsol MultiPhysics is used to calculate the fundamental guided modes and their effective modal indices to calculate the birefringence parameter of the fiber. It should be noted that as seen in Figure 1a, the nonsymmetric arrangement of the air holes and infiltration of chloroform into one of the holes results in a highly asymmetric fiber structure and a large birefringence parameter for the guided modes in the fiber core. The phase of the unheated part of fiber ( $\Phi_1$ ), the heated part of fiber ( $\Phi_2$ ), and the phase difference can be calculated as follows [4]:

$$\Phi_1 = \frac{2\pi B(\lambda, T_0)(L - L_1)}{\lambda} \tag{5}$$

$$\Phi_2 = \frac{2\pi B(\lambda, T)(L_1)}{\lambda} \tag{6}$$

$$\Delta\Phi = \frac{2\pi\Delta B L}{\lambda} \tag{7}$$

where  $\Delta B$  is the birefringence variation between two temperatures,  $L_1$  is the liquid infiltrated length of the fiber sensing element, and  $\lambda$  is the excitation wavelength. Under a phase matching condition ( $\phi_1 + \phi_2 = 2m\pi$ ), the transmission spectrum of the fiber reaches a minimum, and the interference dip wavelength appears. The transmission spectrum ( $SP_{trans}$ ) of the fiber loop (and proposed PCF sensor) in the Sagnac interferometer is a cosine function of wavelength, fiber birefringence, temperature, and length of the fiber, given by [4]:

$$SP_{trans} = (1 - \cos(\phi_1 + \phi_2)) \times 0.5 \quad (8)$$

It should be noted that the most important parameter in a Sagnac interferometer temperature sensor is the spacing between dip wavelengths due to different temperatures. One can find a dip wavelength shift caused by temperature variations for a certain excitation wavelength [4]:

$$\Delta\lambda_{dip} = \lambda \frac{\Delta B}{B} \frac{L_1}{L} \quad (9)$$

where  $L$  is the total length of the fiber. In the experiments, the whole sensing element or a part of the fiber loop can be placed in a temperature chamber to study the sensitivity, resolution, and detection range of the sensor. Here, we assume that the whole length of the sensing element is inside the temperature chamber for simplicity. As seen in Equation (9), the ultimate parameter that determines the dip wavelength shift and consequently the sensitivity for a certain temperature change is the birefringence sensitivity, which can be defined as the ratio of birefringence variations and the base birefringence ( $\Delta B/B$ ). This parameter is studied in detail in the next section, where we show how we can optimize our design to maximize this parameter.

### 3. Design of the Sensor and Birefringence Sensitivity

Fiber birefringence and the sensitivity of the birefringence to the variations in the temperature are the most important parameters in a Sagnac interferometer that is based on optical fibers. Therefore, we studied multiple different structures, designs, and dimensions to find an optimized design with a large birefringence at a specific temperature ( $B_{@T_0}$ ), a large birefringence variation between two temperatures ( $\Delta B = B_{@T_1} - B_{@T_0}$ ), and as a result, a large birefringence sensitivity for a large range of temperatures ( $\Delta B/B$ ). In Figure 4, we demonstrate a number of these designs, their birefringence sensitivity, and the corresponding electrical field distributions for the fundamental guided mode with an x-polarized excitation at 1200 nm. It should be noted that the proposed final structure has six different design parameters: the location of liquid holes (and type of liquid), hole diameter  $d$ , two modified-position holes with diameters  $D_1$  and  $D_2$ , modified-location hole pitch  $\Lambda_1$ , and nonmodified-location hole pitch  $\Lambda_2$ . As mentioned before, chloroform has the highest TOC and a low refractive index, and therefore it is the preferable choice for our temperature sensing application. As expected, the fiber does not show any significant birefringence sensitivity (close to 0%) without chloroform infiltration in Figure 4a. Interestingly, filling all the holes with chloroform does not increase the birefringence sensitivity of the PCF (sensitivity still close to 0%). The birefringence sensitivity increases as we infiltrate only the two airholes close to the core of the fiber (Figure 4b), but the sensitivity (12.5%) is not large enough to guarantee a significant difference in the transmission spectra in a Sagnac interferometer.

We tried to introduce asymmetries in the fiber cross section by changing the size of two adjacent airholes to the fiber core to improve the birefringence sensitivity (Figure 4c). The birefringence sensitivity improved from 12.5% to 16.6%. As seen in Figure 4d, by infiltrating only one of the holes the birefringence sensitivity increases from 16.6% to 28.6% which is considerably a large sensitivity for a given temperature variation. By choosing the optimized design (Figure 4d), we then studied the relationship between fiber birefringence and the ambient temperature with a 1200 nm laser excitation. As seen in Figure 5, there is an almost linear relationship ( $R^2 = 0.989$ ) between the birefringence

parameter and temperature in our proposed fiber. The birefringence decreases from  $7.7 \times 10^{-4}$  to  $2.6 \times 10^{-4}$  with an increase in the temperature from 15 to 45 °C.

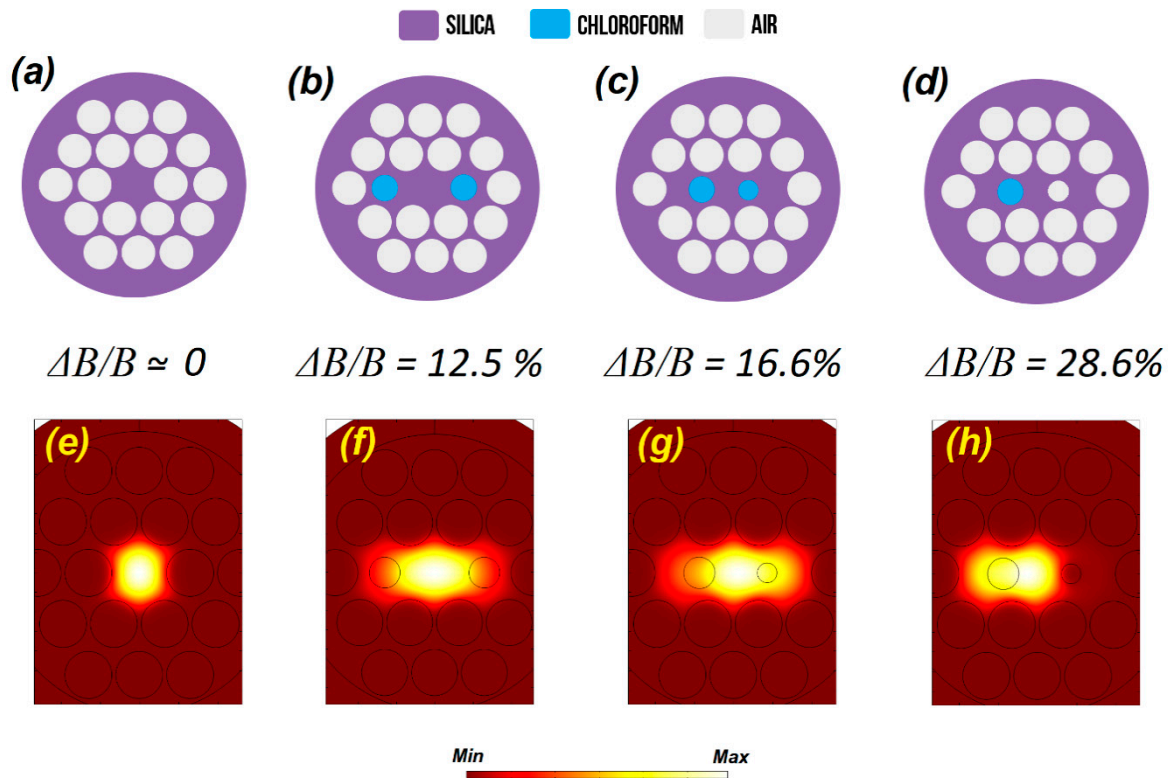


**Figure 4.** (a–d) Birefringence sensitivity and cross section of chloroform-filled PCFs with different design and infiltration patterns. (e–h) The corresponding electrical field distribution of the fundamental guided mode in the PCF core for an x-polarized light excitation at 1200 nm.

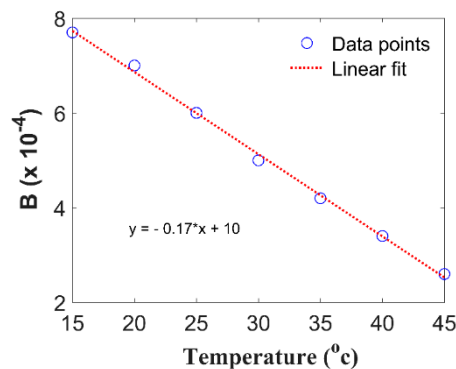


**Figure 5.** Fiber birefringence as a function of temperature for the optimized design with  $d = 1.2 \mu\text{m}$ ,  $\Lambda_1 = 2.6 \mu\text{m}$ ,  $\Lambda_2 = 3.9 \mu\text{m}$ ,  $D_1 = 0.8 \mu\text{m}$ , and  $D_2 = 0.5 \mu\text{m}$ .

Next, we studied the role of the design parameters on birefringence sensitivity in detail. It should be noted that the birefringence sensitivity has a direct impact on the dip wavelength shift and the overall temperature sensitivity of the fiber in the Sagnac interferometer, as demonstrated in Equation (9). We started with the role of spacing between two adjacent holes to the fiber core in Figure 6a. As expected, the location and spacing of the holes is crucial to ensure we have an optical fiber with high birefringence sensitivity. The optimized value for spacing between the adjacent holes to the fiber core is 1.5 according to the simulations; we therefore utilized this ratio in the proposed optimized design by choosing  $\Lambda_1 = 2.6 \mu\text{m}$  and  $\Lambda_2 = 3.9 \mu\text{m}$ . It is important to mention that by choosing a different ratio between holes spacing—for example, 1 instead of 1.5—the sensitivity decays very fast to values smaller than

10%. The role of airhole dimension (Figure 6b), the size of the larger adjacent hole to the core (Figure 6c), and the size of the smaller adjacent hole to the core (Figure 6d) are also studied. To maximize birefringence sensitivity, we chose design parameters that correspond to the maximum sensitivity in each case. The optimized design parameters in the proposed fiber (which are determined after a significant amount of trial and error) are  $d = 1.2 \mu\text{m}$ ,  $\Lambda_1 = 2.6 \mu\text{m}$ ,  $\Lambda_2 = 3.9 \mu\text{m}$ ,  $D_1 = 0.8 \mu\text{m}$ , and  $D_2 = 0.5 \mu\text{m}$ . Interestingly, the small variations (on the orders of a  $0.01 \mu\text{m}$ ) in the airhole dimensions do not have a major effect on the birefringence sensitivity of the fiber as demonstrated in Figure 6b–d. In summary, Figure 6 shows the importance of the location and size of two adjacent holes to the fiber core in the birefringence sensitivity of the proposed PCF. It should be noted that the proposed design has an overall good tolerance to fabrication-induced imperfections, especially imperfections related to the minor variations in the hole size, as demonstrated in Figure 6.

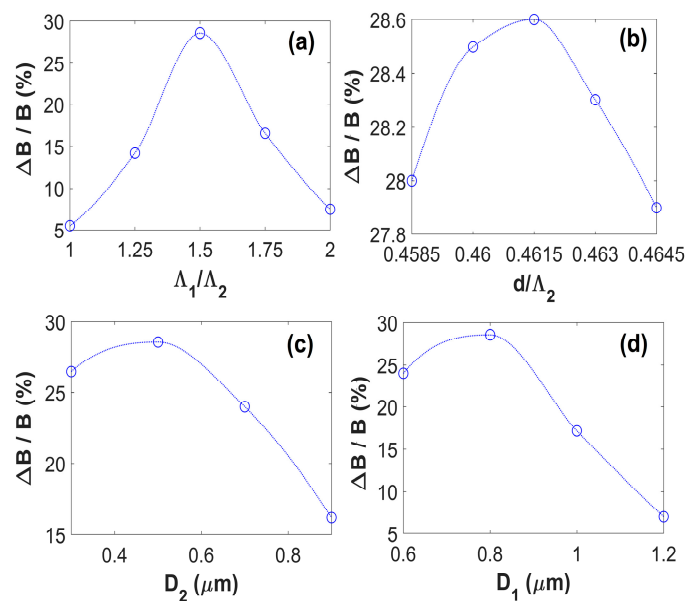


**Figure 6.** Birefringence sensitivity as a function of different design parameters: (a) hole pitch ratio where  $d = 1.2 \mu\text{m}$ ,  $\Lambda_2 = 3.9 \mu\text{m}$ ,  $D_1 = 0.8 \mu\text{m}$ , and  $D_2 = 0.5 \mu\text{m}$ ; (b) hole ratio where  $\Lambda_1 = 2.6 \mu\text{m}$ ,  $\Lambda_2 = 3.9 \mu\text{m}$ ,  $D_1 = 0.8 \mu\text{m}$ , and  $D_2 = 0.5 \mu\text{m}$ ; (c) unfilled central hole diameter where  $d = 1.2 \mu\text{m}$ ,  $\Lambda_1 = 2.6 \mu\text{m}$ ,  $\Lambda_2 = 3.9 \mu\text{m}$ ,  $D_1 = 0.8 \mu\text{m}$ ; (d) filled-hole diameter where  $d = 1.2 \mu\text{m}$ ,  $\Lambda_1 = 2.6 \mu\text{m}$ ,  $\Lambda_2 = 3.9 \mu\text{m}$ , and  $D_2 = 0.5 \mu\text{m}$ .

#### 4. Performance Analysis

By using the optimized design parameters, we analyzed the temperature sensing performance of the proposed fiber in a Sagnac interferometer. As seen in Figure 7, by increasing the temperature from 15 to 35 °C, the transmission dip wavelength blueshifts from 1155 to 629 nm. While the variations of the transmission spectra are significant within the 15–35 °C window, the variations are significantly reduced outside this temperature range. We also studied the role of fiber length on the transmission spectra in Figure 8 at a constant temperature of 30 °C. It is clear that by increasing the fiber length from 1.5 to 15 mm, the number of transmission dips increases significantly (from 1 to 6 between 600 and 1200 nm). The increase in the number of transmission dips can make the detection of the dip wavelength more difficult and challenging, and therefore we chose 1.5 mm as the optimized fiber length in all of the calculations.

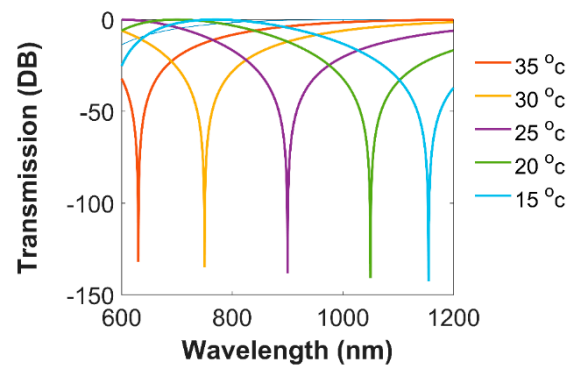


**Figure 7.** Transmission spectra of the Sagnac interferometer optical fiber sensor as a function of wavelength for different temperatures.

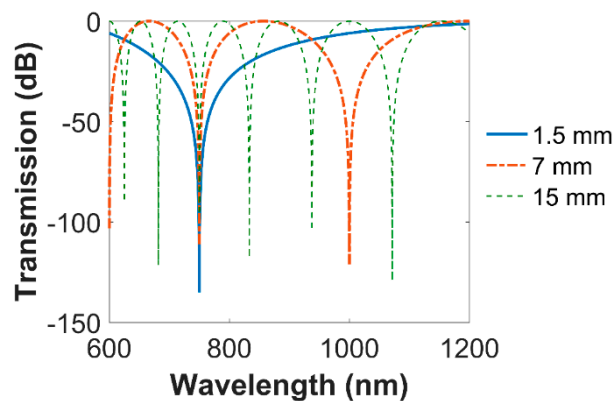


**Figure 8.** Transmission spectra of the Sagnac interferometer optical fiber sensor as a function of wavelength for different fiber lengths.

Finally, we examined the variations in the dip wavelength of the proposed sensor as a function of the ambient temperature. According to Figure 9a, the proposed sensor consists of two main regions. The first region is a linear region (15–35 °C), in which the sensor is highly sensitive to any changes in the ambient temperature, and the relationship between dip wavelength and temperature is almost linear ( $R^2 = 0.986$ ), as seen in Figure 9b. In optical fiber-based sensors, in addition to the working range, usually sensitivity and resolution are the most important parameters that determine the merit of the sensing component [21,22]. The temperature sensitivity and temperature resolution of the proposed sensor can be calculated from [21,22]:

$$S \text{ (nm/C)} = \frac{\Delta\lambda_{dip}}{\Delta T} \tag{10}$$

$$R \text{ (C)} = \frac{\Delta T \times \Delta\lambda_{min}}{\Delta\lambda_{dip}} \tag{11}$$

where  $\Delta T$  is the difference between the minimum and maximum ambient temperatures, and  $\Delta\lambda_{min}$  is the minimum spectral resolution of the detector. The average linear temperature sensitivity of the proposed sensor in the linear region is 17.53 nm/°C, which is higher than that of the most recent fiber-optic-based Sagnac interferometer temperature sensors with liquid infiltration. Considering a minimum spectral resolution of 0.01 nm in the detector [6], an average resolution of  $5.7 \times 10^{-4}$  °C is also achieved. In particular, the proposed sensor has a large linear sensitivity of 25.6 nm/°C between 20 and 30 °C. In the second region (larger than 35 °C or smaller than 15 °C) there is no linear relationship between dip wavelength and temperature. The temperature sensitivity in the nonlinear region also decreases significantly comparing to the linear region.

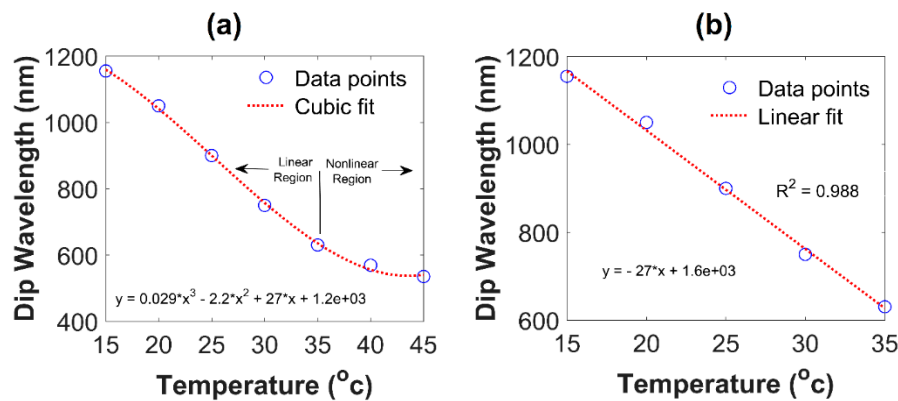


**Figure 9.** Dip wavelength of transmission spectra of the Sagnac interferometer optical fiber sensor as a function of ambient temperature for (a) linear and nonlinear regions with a temperature range of 15–45 °C and (b) a linear region with a temperature range of 15–35 °C.

In Table 1, we compared the performance of our proposed temperature sensor with other similarly reported temperature sensors based on liquid-filled optical fibers. It is clear that our proposed chloroform-filled sensor has a higher spectral sensitivity and resolution comparing to other previously reported structures in the literature. Furthermore, the operation range (linear regime) of our sensor is slightly higher than the previously reported Sagnac-interferometer-based optical fiber sensors (30 nm in our case compared to 17 nm in [6], 26 nm in [7], and 10 nm in [4]). It should be mentioned that due to the limitation in detection range of small-size optical detectors, it is not possible to improve the sensitivity and detection range (at the same time) over a certain limit without compromising the cost and size of the sensor. The current small-size cost-effective optical detectors are based on ultraviolet–visible spectroscopy (UV–Vis), which usually cannot detect optical signals below 200 nm and over 1200 nm.

**Table 1.** The temperature sensing performance of a water-filled PCF in [6], alcohol-filled PCF in [7], toluene-filled PCF in [4], and the proposed chloroform-filled PCF in a Sagnac interferometer.

	Ref [6]	Ref [7]	Ref [4]	This Work
Infiltration Liquid	Water	Alcohol	Toluene	Chloroform
Maximum Birefringence	$1.999 \times 10^{-4}$	$3.5 \times 10^{-4}$	$8.68 \times 10^{-5}$	$7.7 \times 10^{-4}$
Average Sensitivity (nm/°C)	2.58	6.6	11	17.53
Temperature Range (°C)	25–42	8–34	20–30	15–35
Resolution (°C)	$4 \times 10^{-3}$	-	-	$5.7 \times 10^{-4}$

Comparing to other temperature sensing technologies like thermocouples, thermistors, and resistance temperature detectors, our proposed design offers important advantages, including possible remote sensing, possible distributed sensing, immunity to electromagnetic waves interference, and higher detection limits (resolutions). Furthermore, we should emphasize that optical fiber-based temperature sensors can enable temperature sensing in harsh environments, as the sensing element is a fiber that can easily reach hard-to-reach points for temperature sensing. Examples of harsh environments that an optical fiber-based temperature sensor can be a preferable option are inflammable atmospheres, all-electrical aircraft batteries, ocean floors, and oil pipelines [23,24].

### 5. Conclusions

A new design of an ultrasensitive Sagnac-interferometer-based optical fiber temperature sensor was theoretically and numerically proposed here. Using the finite element method, the modal birefringence of the fiber under different ambient temperatures and the birefringence sensitivity of the

fiber were numerically investigated while one of the airholes was infiltrated with liquid chloroform. A large birefringence sensitivity of almost 29% to a 10 °C temperature variation was reported for the optimized fiber design. The performance of the proposed optical fiber in a temperature sensor Sagnac interferometer is studied in detail, and an average linear temperature sensitivity of 17.53 nm/°C with an average resolution of  $5.7 \times 10^{-4}$  °C was achieved over a temperature range of 20 °C (15 °C to 45 °C).

**Author Contributions:** Conceptualization, Y.E.M.; Methodology, Y.E.M. and C.L.; Software, A.A.; Validation, V.D.; Formal Analysis, Y.E.M. and A.A.; Data Curation, Y.E.M. and V.D.; Writing-Original Draft Preparation, Y.E.M.; Writing-Review & Editing, Y.E.M. and A.A. and C.L.; Visualization, Y.E.M. All authors have read and agreed to the published version of the manuscript.

**Funding:** This research received no external funding.

**Acknowledgments:** Y.E.M. acknowledges the support of Dalhousie University for providing the resources to perform this research, and C.L. acknowledges the support of the National Natural Science Foundation of China and the National Key Research and Development Program of China.

**Conflicts of Interest:** The authors declare no conflict of interest.

## References

1. Bowden, C.M.; Zheltikov, A.M. Nonlinear optics of photonic crystals introduction. *J. Opt. Soc. Am. B* **2002**, *19*, 2046–2048. [[CrossRef](#)]
2. Pathak, A.K.; Singh, V.K. A wide range and highly sensitive optical fiber pH sensor using polyacrylamide hydrogel. *Opt. Fiber Technol.* **2017**, *39*, 43–48. [[CrossRef](#)]
3. Wadsworth, W.; Knight, J.; Birks, T. State-of-the-art photonic crystal fiber. *Opt. Photonics News* **2012**, *23*, 24–31. [[CrossRef](#)]
4. Monfared, Y.E.; Liang, C.; Khosravi, R.; Kacerovska, B.; Yang, S. Selectively toluene-filled photonic crystal fiber Sagnac interferometer for temperature sensing applications. *Results Phys.* **2019**, *13*, 102297. [[CrossRef](#)]
5. Ahmadian, A.; Monfared, Y.E. Chalcogenide-tellurite composite photonic crystal fiber: Extreme non-linearity meets large birefringence. *Appl. Sci.* **2019**, *9*, 4445. [[CrossRef](#)]
6. Cui, Y.; Shum, P.; Hu, D.; Wang, G.; Humbert, G.; Dinh, X. Temperature sensor by using selectively filled photonic crystal fiber Sagnac interferometer. *IEEE Photonics J.* **2012**, *4*, 1801–1808. [[CrossRef](#)]
7. Qian, W.; Zhao, C.; He, S.; Dong, X.; Zhang, S.; Zhang, Z.; Jin, S.; Guo, J.; Wei, H. High-sensitivity temperature sensor based on an alcohol-filled photonic crystal fiber loop mirror. *Opt. Lett.* **2011**, *36*, 1548–1550. [[CrossRef](#)]
8. Lu, Y.; Wang, M.; Hao, C.; Zhao, Z.; Yao, J. Temperature sensing using photonic crystal fiber filled with silver nanowires and liquid. *IEEE Photonics J.* **2014**, *6*, 1–7. [[CrossRef](#)]
9. Han, T.; Liu, Y.; Wang, Z.; Guo, J.; Wu, Z.; Wang, S.; Li, Z.; Zhou, W. Unique characteristics of a selective-filling photonic crystal fiber Sagnac interferometer and its application as high sensitivity sensor. *Opt. Express* **2013**, *21*, 122–128. [[CrossRef](#)]
10. Vera, E.; Cordeiro, C.; Torres, P. Highly sensitive temperature sensor using a Sagnac loop interferometer based on a side-hole photonic crystal fiber filled with metal. *Appl. Opt.* **2017**, *56*, 156–162. [[CrossRef](#)]
11. Sasaki, M.; Ando, T.; Nogawa, S.; Hane, K. Direct photolithography on optical fiber end. *Jpn. J. Appl. Phys.* **2002**, *41*, 4350–4355. [[CrossRef](#)]
12. Huang, Y.; Xu, Y.; Yariv, A. Fabrication of function microstructured optical fibers through a selective-filling technique. *Appl. Phys. Lett.* **2005**, *85*, 5182–5184. [[CrossRef](#)]
13. Liu, J.; Cheng, T.; Yeo, Y.; Wang, Y.; Xue, L.; Xu, Z.; Wang, D. Light beam coupling between standard single mode fibers and highly nonlinear photonic crystal fibers based on the fused biconical tapering technique. *Opt. Express* **2009**, *17*, 3115–3123. [[CrossRef](#)] [[PubMed](#)]
14. Martínez-Manuel, R.; May-Arrijo, D.A.; Acevedo-Mijangos, J.; Domínguez-Cruz, R.F.; López-Cortés, D.; Torres-Cisneros, M. Ultra-high sensitivity temperature sensor using a fiber loop mirror based on a water-filled asymmetric two-hole fiber. *IEEE Sens.* **2020**. [[CrossRef](#)]
15. Pilla, V.; Munin, E.; Gesualdi, M.R.R. Measurement of the thermo-optic coefficient in liquids by laser-induced conical diffraction and thermal lens technique. *J. Opt. A Pure Appl. Opt.* **2009**, *11*, 105201. [[CrossRef](#)]

16. Kim, Y.H.; Park, S.J.; Jeon, S.; Ju, S.; Park, C.; Han, W.; Lee, B. Thermo-optic coefficient measurement of liquids based on simultaneous temperature and refractive index sensing capability of a two-mode fiber interferometric probe. *Opt. Express* **2012**, *20*, 23744–23754. [[CrossRef](#)]
17. Monfared, Y.E.; Ponomarenko, S.A. Extremely nonlinear carbon-disulfide-filled photonic crystal fiber with controllable dispersion. *Opt. Mater.* **2019**, *88*, 406–411. [[CrossRef](#)]
18. Monfared, Y.E.; Hajati, M.; Liang, C.; Yang, S.; Qasymeh, M. Quasi-D-shaped fiber optic plasmonic biosensor for high-index analyte detection. *IEEE Sens.* **2019**. [[CrossRef](#)]
19. Malitson, I.H. Interspecimen comparison of the refractive index of fused silica. *J. Opt. Soc. Am.* **1965**, *55*, 1205–1208. [[CrossRef](#)]
20. Ayyanar, N.; Vasanth, R.; Rajab, J.; Vigneswaran, D.; Lakshmi, B.; Sumathia, M.; Porseziand, K. Highly efficient compact temperature sensor using liquid infiltrated asymmetric dual elliptical core photonic crystal fiber. *Opt. Mater.* **2017**, *64*, 482–574. [[CrossRef](#)]
21. Monfared, Y.E. Refractive index sensor based on surface plasmon resonance excitation in a d-shaped photonic crystal fiber coated by titanium nitride. *Plasmonics* **2020**, *15*, 535–542. [[CrossRef](#)]
22. Rifat, A.A.; Mahdiraji, G.A.; Sua, Y.M.; Ahmed, R.; Shee, Y.G.; Adikan, F.R.M. Highly sensitive multi-core flat fiber surface plasmon resonance refractive index sensor. *Opt. Express* **2016**, *24*, 2485–2495. [[CrossRef](#)] [[PubMed](#)]
23. Vázquez, C.; Tapetado, A.; Pinzón, P.J.; Montero, D.S.; López-Cardona, J.D.; Contreras, P.; Zubia, J. Temperature sensing using optical fibers in harsh environments. In Proceedings of the 19th International Conference on Transparent Optical Networks (ICTON), Girona, Spain, 2–6 July 2017; pp. 1–4.
24. Zhang, M.; Ma, X.; Wang, L.; Lai, S.; Zhou, H.; Zhao, H.; Liao, Y. photonic sensors review progress of optical fiber sensors and its application in harsh environment. *Photonic Sens.* **2011**, *1*, 84–89. [[CrossRef](#)]



© 2020 by the authors. Licensee MDPI, Basel, Switzerland. This article is an open access article distributed under the terms and conditions of the Creative Commons Attribution (CC BY) license (<http://creativecommons.org/licenses/by/4.0/>).